Thermal radiation and inclusive production in the Kharzeev-Levin-Nardi model for ion-ion collisions

E. Gotsman[1,*] and E. Levin[1,2,†]

[1]*Department of Particle Physics, School of Physics and Astronomy,*
Raymond and Beverly Sackler Faculty of Exact Science, Tel Aviv University, Tel Aviv 69978, Israel
[2]*Departemento de Física, Universidad Técnica Federico Santa María,*
and Centro Científico-Tecnológico de Valparaíso, Avenida Espana 1680, Casilla 110-V, Valparaíso, Chile

We show that in order to obtain a successful description of the transverse momenta distribution for charged particles in ion-ion collisions, one must include a thermal emission term. The temperature of this emission T_{th} turns out to be proportional to the saturation scale, $T_{\text{th}} = 1.8 Q_s / 2\pi$. The formalism for the calculation of the transverse momenta spectra in color glass condensate/saturation approach is developed, in which two stages of the process are seen: creation of the color glass condensate, and hadronization of the gluon jets. Our calculations are based on the observation that even for small values of p_T, the main contribution in the integration over the dipole sizes stems from the kinematic region in the vicinity of the saturation momentum, where theoretically, we know the scattering amplitude. Nonperturbative corrections need to be included in the model of hadronization. This model incorporates the decay of a gluon jet with effective mass $m_{\text{eff}}^2 = 2 Q_s \mu_{\text{soft}}$ where μ_{soft} denotes the soft scale, with the fragmentation functions at all values of the transverse momenta. We use the Kharzeev-Levin-Nardi model which, provides a simple way to estimate the cross sections for the different centrality classes. Comparing the results of this paper with the transverse distribution in the proton-proton scattering, we see two major differences. First, a larger contribution of the thermal radiation term is needed, in accord with higher parton densities of the produced color glass condensate. Second, even changing the model for the hadronization, without a thermal radiation term, we fail to describe the p_T spectrum. Consequently, we conjecture that the existence of the thermal radiation term is independent of the model of confinement.

I. INTRODUCTION

In this paper we continue to discuss the processes of multi-particle generation at high energy, in the framework of the color glass condensate (CGC)/saturation approach (see Ref. [1] for the review). The main ideas of our approach have been discussed in our paper (see Ref. [2]) for hadron-hadron scattering at high energies. Here, we consider heavy ion collisions in which, we believe, the distinctive features of the CGC/saturation approach manifest themselves in the clearest way. For theoretical descriptions of these processes we have to develop a nonperturbative approach, since these processes occur at long distances. In particular, we have to deal with the

unsolved problem of the confinement of quarks and gluons. Fortunately, in the framework of the CGC/saturation approach, the most basic features of the processes of the multiparticle generation stem from the production of the new phase of QCD: the dense system of partons (gluons and quarks) with a new characteristic scale: saturation momentum $Q_s(W)$, which increases as a function of energy W [3–5]. In ion-ion collisions the new phase of QCD is produced with a larger density than in hadron-hadron scattering, and we believe, that the essential properties of this phase will manifest themselves in a clear way. However, the transition from this system of partons to the measured state of hadrons, is still an unsolved problem.

Due to our lack of theoretical understanding of the confinement of quarks and gluons, at the moment, we need to use a pure phenomenological input for the long distance nonperturbative physics. In particular, we wish to use phenomenological fragmentation functions. Hence, our model for confinement is that the parton (quark or gluon) with the transverse momenta of the order of Q_s decays into hadrons according to the given fragmentation functions. Experimental data supports this model of hadronization,

*gotsman@post.tau.ac.il
†leving@tauex.tau.ac.il,eugeny.levin@usm.cl

which provides the foundation of all Monte Carlo simulation programs, and leads to descriptions of the transverse momenta distribution of the hadrons, at the LHC energies. As an example, we refer to Ref. [6], which shows that next-to-leading order QCD calculations with formation of the hadrons in accord with the fragmentation functions ([7]), is able to describe the transverse momentum spectra, for the LHC range of energies. In a sense, at present, this model is the best that we can propose to describe multihadron production.[1]

The space-time picture of the high energy interaction in the CGC/saturation approach, is as follows: The parton configuration in QCD is formed long before the interaction at distances R_A/x, where R_A denotes the nucleus radius, and x the fraction of longitudinal momentum carried by the parton which interacts with the target. However, before the collision, the wave function of this partonic fluctuation is the eigenfunction of the Hamiltonian and, therefore, the system has zero entropy. The interaction with the target of size R_A destroys the coherence of the parton wave function of the projectile. The typical time, which is needed for this, is of the order of $\Delta t \propto R_A$, and is much smaller than the lifetime of all faster partons in the fluctuation. Hence, this interaction can be viewed as a rapid quench of the entangled partonic state [9] with substantial entanglement entropy. After this rapid quench, the interaction of the gluons change the Hamiltonian. Since in the CGC/saturation approach all partons with rapidity larger than that of a particular gluon y_i, live longer than this parton, so they can be considered to be the source of the classical field that emits this gluon. It has been shown that after the quench, the fast gluons create the longitudinal chromoelectrical background field. Moving in this field the gluon accelerates and emits gluons which have the thermal distribution (the first term of Eq. (2) below) [10–12]. The temperature of this distribution is intimately related to the saturation momentum, which provides the only dimensional scale in the color glass condensate. It determines both the strength of the longitudinal fields and the ultraviolet cutoff on the quantum modes, resolved by the collision. It turns out [10–14] that

$$T_{\text{th}} = c\frac{Q_s}{2\pi} \qquad (1)$$

with the semiclassical estimates [11] for the constant $c = 1.2$.

The appearance of a thermal emission in a high energy proton-proton collision is a remarkable feature of the interaction, since the number of the secondary interactions

in proton-proton collisions is rather low, and cannot provide the thermalization due to the interaction in the final state. The origin of thermal radiation in the framework of the CGC approach was clarified a decade ago [10,11,13,14] and, recently, the new idea that the quantum entanglement is at the origin of the parton densities, has been added to these arguments [9].

The goal of this paper is to revisit the process of inclusive production in the CGC/saturation approach, for more thorough consideration, and to show that the thermal term with the temperature given by Eq. (1), is needed for describing the experimental data for ion-ion collisions at high energies. At first sight, it looks as we are pushing at an open door, since it has been shown [12,15–19] that the experimental data [6,20–24] at high energy both for hadron-hadron and ion-ion scattering, can be described as the sum of two terms:

$$\frac{d\sigma}{dy\, d^2 p_T} = \underbrace{A_{\text{therm}} e^{-\frac{m_T}{T_{\text{th}}}}}_{\text{thermal radiation}} + A_{\text{hard}} \underbrace{\frac{1}{(1 + \frac{m_T^2}{T_h^2 n})^n}}_{\text{hard emission}} \qquad (2)$$

with

$$T_{\text{th}} = 0.098\left(\sqrt{\frac{s}{s_0}}\right)^{0.06} \text{GeV};$$

$$T_{\text{h}} = 0.409\left(\sqrt{\frac{s}{s_0}}\right)^{0.06} \text{GeV}; \qquad (3)$$

The first term in Eq. (2) is the desired thermal radiation, while the second term describes hadron production in the hard processes, showing the powerlike decrease at high p_T. The same dependence on energy of both T_{th} and T_{h} supports the main idea of CGC, i.e., both parameters are related to the saturation momentum (Q_s). However, it turns out that this dependence differs from the saturation scale $Q_s \propto \left(\sqrt{\frac{s}{s_0}}\right)^\lambda$.

The value of λ can be calculated theoretically and measured experimentally. The leading order QCD evaluation leads to $\lambda = 4.9\bar{\alpha}_S$, where $\bar{\alpha}_S$ denotes the running QCD coupling. Plugging in a reasonable estimate for $\bar{\alpha}_S(Q_s) \approx 0.2$, λ turns out to be large, about 0.8-1. The phenomenological description of the hard processes both for nucleus interactions [25] and deep inelastic scattering (DIS) (see Ref. [26] and references therein), give the value of $\lambda = 0.2$–0.24. Thus, in the CGC approach we expect

$$T_{\text{th}} \propto T_{\text{h}} \propto \left(\sqrt{\frac{s}{s_0}}\right)^{\lambda/2} \sim \left(\sqrt{\frac{s}{s_0}}\right)^{0.1-0.112}.$$

Hence, in spite of the fact that Eqs. (2) and (3) show that both temperatures have dependence on energy in accord with the CGC result, this dependence contradicts the

---

[1]We have to mention, that actually the model of hadronization with given fragmentation function describes the experimental data at large values of p_T ($p_T \geq 3$ GeV [7] and $p_T \geq 5$ GeV [8]). In our model of the hadronization we assume that we can describe the data with the fragmentation function at any value of p_T. We will demonstrate that such a description is possible.

CGC prediction. Especially, the different Q_s energy dependence in the second term of Eq. (2), which corresponds to the contribution of the hard processes, looks strange if not wrong, since the CGC approach to the hard processes has been confirmed both theoretically and experimentally, and we know that the typical scale in these processes, is the saturation momentum. The second remark is related to the value of the hard contribution. In the CGC approach it should be calculated theoretically, and not be determined by a fitting procedure.

II. INCLUSIVE PRODUCTION IN CGC/ SATURATION APPROACH FOR ION-ION COLLISON

A. General formulas

The general formula for the gluon jet production in ion-ion collisions in the CGC/saturation approach, has the following form (see Ref. [27] for the proof):

$$\frac{d\sigma_G}{dy d^2 p_T} = \frac{2C_F}{\alpha_s (2\pi)^4} \frac{1}{p_T^2} \int d^2 r e^{i\mathbf{p}_T \cdot \mathbf{r}}$$

$$\times \int d^2 b \nabla_T^2 N_G^{A_1}(y_1 = \ln(1/x_1); r, b)$$

$$\times \int d^2 b' \nabla_T^2 N_G^{A_2}(y_2 = \ln(1/x_2); r, b'), \quad (4)$$

where $N_G^{A_i}(y_1 = \ln(1/x_1); r, b)$ can be found from the amplitude of the dipole-nucleus scattering $N^{A_i}(y_i = \ln(1/x_i); r, b)$:

$$N_G^{A_i}(y_i = \ln(1/x_i); r, b)$$
$$= 2N^{A_i}(y_i = \ln(1/x_i); r, b) - (N^{A_i}(y_i = \ln(1/x_i); r, b))^2$$
$$(5)$$

where r denotes the size of the dipole, b its impact parameter, and

$$x_1 = \frac{p_T}{W} e^y; \qquad x_2 = \frac{p_T}{W} e^{-y}; \qquad (6)$$

where y denotes the rapidity of the produced gluon in center of mass frame and W the c.m.f. energy of the collision. In this paper we consider the gluon production at $y = 0$. $C_F = (N_c^2 - 1)/2N_c$ and $\bar{\alpha}_S = \alpha_S N_c / \pi$ with the number of colors equals N_c. α_S denotes the running QCD coupling, ∇_T^2 the Laplace operator with respect to r, it is equal to $\nabla_T^2 = \frac{1}{r} \frac{d}{dr}(r \frac{d}{dr})$.

In our paper [2] we found that the main contribution at high energies stems from the specific kinematic region in the vicinity of the saturation scale. Indeed, at high energies and sufficiently small values of p_T the dipole amplitudes are in the saturation region, where the parton densities are large and the dipole scattering amplitude displays geometric scaling behavior, being a function of only one variable: $\tau = r Q_s(W, b)$ [28–30]. Deep in the saturation

region the dipole amplitude tends to approach 1, but $\nabla_T^2 N_G^{A_1}(y_1 = \ln(1/x_1); r, b) \xrightarrow{\tau \gg 1} 0$. Consequently the main contribution in Eq. (4) stems from the kinematic region where $\tau \sim 1$ or, in other words, from the vicinity of the saturation scale. The most attractive features of this observation is the fact that we know theoretically the behavior of the scattering amplitude in this region. It has the form (Ref. [31]):

$$N(y_i = \ln(1/x_i); r, b) = N_0(r^2 Q_s(A, Y, b))^{\bar{\gamma}} = N_0(\tau)^{2\bar{\gamma}}$$
$$(7)$$

where $\bar{\gamma} = 1 - \gamma_{cr}$ and $\gamma_{cr} = 0.37$ in the leading order is the solution to the equation [1]:

$$\frac{d\chi(\gamma_{cr})}{d\gamma_{cr}} = -\frac{\chi(\gamma_{cr})}{1 - \gamma_{cr}}. \qquad (8)$$

$\chi(\gamma)$ is given by

$$\chi(\gamma) = 2\psi(1) - \psi(\gamma)) - \psi(1 - \gamma). \qquad (9)$$

Note that $\omega = \bar{\alpha}_S \chi(\gamma)$ is the eigenvalue of the Balitsky-Fadin-Kuraev-Lipatov (BFKL) equation [32].

The saturation momentum $Q_s(A, Y, b)$ has the following dependence on energy [3–5]

$$Q_s(A, Y, b) = Q_s(A, Y = Y_0, b) e^{\lambda(Y - Y_0)} \qquad (10)$$

where $\lambda = \bar{\alpha}_S \chi(\gamma_{cr})/(1 - \gamma_{cr})$ in the LO of perturbative QCD. We will discuss below the dependence of the saturation momentum on the number of nucleons in a nucleus [A in Eq. (7) and in Eq. (10)]. It should be stressed that Eq. (7) together with Eq. (10) gives the correct behavior $N \propto \exp(-\mu b)$ of the scattering amplitude at large impact parameter, which is determined by the nonperturbative behavior of the saturation momentum at the initial energy (Y_0). It should be compared with the general case, for which at the moment we are not able to modify the main equations in a such way to obtain this behavior [33]. Note, that we can find N_G of Eq. (5) only if we know the impact parameter behavior of the scattering amplitude.

Hence, we conclude that $\nabla_T^2 N_G^{A_1}(y_1 = \ln(1/x_1); r, b)$ and $\nabla_T^2 N_G^{A_1}(y_2 = \ln(1/x_2); r, b)$ in Eq. (4), as well as the integral over r, can be calculated in the framework of CGC/ saturation approach, and there is no need to introduce the nonperturbative corrections due to the unknown physics at long distances (see Refs. [34,35] for example) in the dipole scattering amplitude. However, plugging the scattering amplitude of Eq. (7) in Eq. (4), one can see that $\int d^2 r e^{i\mathbf{p}_T \cdot \mathbf{r}} \int d^2 b \nabla_T^2 N_G^{A_1} \int d^2 b' \nabla_T^2 N_G^{A_2}$ is not suppressed at $p_T \to 0$. Therefore, we have $\frac{d\sigma_G}{dy d^2 p_T} \propto 1/p_T^2$. This divergence can only be tamed in the process of hadronization, which has to be treated using a nonperturbative approach to QCD.

At the moment, as has been alluded to in the introduction, we can treat the hadronization only using phenomenological models. Our model consists of two elements. First, every gluon decays into the jet of hadrons with a known fragmentation function:

$$\frac{d\sigma^{\pi}}{dyd^2p_T} = \int_0^1 dx_G \frac{d\sigma_G}{dyd^2p_T}\left(\frac{p_T}{x_{\pi}}\right)D_G^{\pi}(x_{\pi}) \quad (11)$$

We take the fragmentation function D_G^{π} from Ref. [36] which has the form

$$D_G^{\pi}(x^{\pi}) = 2.17z^{\alpha}(1-z)^{\beta}(20(1-z)^{\gamma_1}+1); \quad (12)$$

with $\alpha = 0.899$, $\beta = 1.57$ and $\gamma = 4.91$. It should be stressed, that we assume that Eq. (11) holds for any value of the transverse momenta of gluons, while it is shown that this equation gives a good description of the experimental data for rather large transverse momenta: $p_T > 3$ GeV [7] and $p_T > 5$ GeV [8]. It is not clear, how such a fragmentation function takes into account resonance production, which leads to an enhancement at low momenta, and could affect the value of the thermal term, that we extract from the experimental data. However, the typical p_T, which are essential in our approach, are rather large $p_T \sim Q_s$, these increase with the growth of energy and of the number of participants. Therefore, the discussion of the transverse momenta spectra in the nucleus-nucleus collision provides a possibility to separate the thermal emission term from the emissions of the resonances.

We note that Eq. (4) as well as Eq. (11) lead to a cross section which is proportional to $1/p_T^2$. This behavior results in a logarithmic divergency of the integral over p_T, or in other words gives an infinite number of produced pions at fixed rapidity. The reason for this problem, is that we neglected the mass of the jet of hadrons that stems from the decay of the gluon. The simple estimates [37] give for a gluon with the value of the transverse momentum p_T, the mass of the jet $m_{\text{jet}}^2 = 2p_Tm_{\text{eff}}$, where $m_{\text{eff}} = \sqrt{m^2 + k_T^2 + k_L^2} - k_L$, m is the mass of the lightest hadron in the jet, k_T is its transverse momentum and $k_L \approx k_T$ is the longitudinal momentum of this hadron. Since most pions stem from the decay of ρ-resonances we expect that $m_{\text{eff}} \approx m_{\rho}$.

As we have mentioned in the Introduction, our model for confinement is that of the CGC approach, the typical momentum for the produced gluon is the saturation momentum. Hence, most hadrons are created in the jets with the mass $m_{\text{jet}}^2 = 2Q_sm_{\text{eff}}$. However, for rare gluons with $p_T \gg Q_s$ we still have $m_{\text{jet}}^2 = 2p_Tm_{\text{eff}}$. For numerical estimates we use $m_{\text{jet}}^2 = 2(Q_s\Theta(Q_s - p_T) + p_T\Theta(p_T - Q_s))m_{\text{eff}}$ which has these two limits. $\Theta(x)$ denotes the step function. Using the same idea we replace Eq. (6) by

$$x = \frac{p_T}{W} = \frac{Q_s\Theta(Q_s - p_T) + p_T\Theta(p_T - Q_s)}{W}. \quad (13)$$

Concluding, we see that our model of the hadronization processes includes two ingredients: the fragmentation function of Eq. (12) which gives us the number and p_T distribution of the produced hadron from one gluon; and the replacement $1/p_T^2$ in Eq. (4) by $1/(p_T^2 + m_{\text{jet}}^2)$ with $m_{\text{jet}}^2 = 2(Q_s\Theta(Q_s - p_T) + p_T\Theta(p_T - Q_s))m_{\text{eff}}$.

B. Dipole-nucleon scattering amplitude

For completeness of presentation, in this subsection we give a brief review of our theoretical and phenomenological approach to the contribution of the dipole-nucleon scattering amplitude to the inclusive gluon production, that has been discussed in Ref. [2].

1. $\tau \sim 1$

In the vicinity of the saturation scale the dipole-nucleon scattering amplitude has a general form of Eq. (7), which leads to $N_G(Y; r, b) = 2N(Y; r, b) - N^2(Y; r, b) = 2N_0\tau^{2\bar{\gamma}} - N_0^2\tau^{4\bar{\gamma}}$. After differentiating we obtain:

$$\nabla_T^2 N_G(Y; r, b) = \frac{8\bar{\gamma}^2 N_0(rQ_s)^{2\bar{\gamma}}}{r^2}(1 - 2N_0(rQ_s)^{2\bar{\gamma}})$$
$$= \frac{8\bar{\gamma}^2 N_0\tau^{2\bar{\gamma}}}{r^2}(1 - 2N_0\tau^{2\bar{\gamma}}) \quad (14)$$

2. $\tau > 1$

Inside of the saturation domain we suggest using $N = 1 - \exp(-\phi_0\tau^{2\bar{\gamma}})^2$ which gives

$$\nabla_T^2 N_G(Y; r, b) = \frac{8\bar{\gamma}^2 \phi_0(rQ_s)^{2\bar{\gamma}}}{r^2}(1 - 2\phi_0(rQ_s)^{2\bar{\gamma}})$$
$$\times \exp(-2\phi_0(rQ_s)^{2\bar{\gamma}})$$
$$= \frac{8\bar{\gamma}^2 \phi_0\tau^{2\bar{\gamma}}}{r^2}(1 - 2\phi_0\tau^{2\bar{\gamma}})e^{-2\phi_0\tau^{2\bar{\gamma}}} \quad (15)$$

We need to match this formula with Eq. (14) at $\tau = 1$. For $N_0 \ll 1$ we obtain $\phi_0 = N_0$.

Reference [2], checked that Eq. (15) describes to a fairly good accuracy the exact solution for the nonlinear Balitsky-Kovchegov [38] equation, for the leading twist BFKL kernel. We wish to remind the reader that the scattering amplitude in this kinematic region only gives a small contribution (not more than 15%) to an event at $p_T = 0$.

---

[2]The reasons why we can use this formula for the inclusive production in the saturation region has been discussed in details in Ref. [2]. In this paper, we showed, that we can use this simple formula, which describes the vicinity of the saturation scale, in the entire saturation region, since in $\nabla_T^2 N_G(Y; r, b)$ the region deeply inside of the saturation domain does not contribute.

3. $\tau < 1$

In this region we can safely use the perturbative QCD approach for the scattering amplitude. Therefore, we need to solve the BFKL evolution equation in this region which has the following form:

$$\frac{\partial N(Y;\boldsymbol{x}_{01},\boldsymbol{b})}{\partial Y} = \frac{\bar{\alpha}_S}{2\pi} \int d^2\mathbf{x_2} K(\boldsymbol{x}_{01};\boldsymbol{x}_{02},\boldsymbol{x}_{12})$$
$$\times \left\{ 2N\left(Y;\boldsymbol{x}_{02},\boldsymbol{b}-\frac{1}{2}\boldsymbol{x}_{12}\right) - N(Y;\boldsymbol{x}_{01},\boldsymbol{b}) \right\}$$

(16)

where

$$K(\boldsymbol{x}_{01};\boldsymbol{x}_{02},\boldsymbol{x}_{12}) = \frac{\mathbf{x}_{01}^2}{\mathbf{x}_{02}^2 \mathbf{x}_{12}^2}$$

(17)

$N(Y;\boldsymbol{x}_{01},\boldsymbol{b})$ denotes the dipole scattering amplitude. $\boldsymbol{x}_{01} = \boldsymbol{x}_1 - \boldsymbol{x}_0 \equiv \boldsymbol{r}$ the size of the dipole. The kernel $K(\boldsymbol{x}_{01};\boldsymbol{x}_{02},\boldsymbol{x}_{12})$ describes the decay of the dipole with size x_{01} into two dipoles of size: $\boldsymbol{x}_{02}$ and $\boldsymbol{x}_{12} = \boldsymbol{x}_{01} - \boldsymbol{x}_{02}$. After integrating Eq. (16) over b the equation reduces to the BFKL equation [32] with the eigenfunctions $(r^2)^\gamma$. Therefore, the general solution takes the form:

$$\int d^2 b N(Y;\boldsymbol{x}_{01},\boldsymbol{b}) = \int_{\epsilon-i\infty}^{\epsilon+i\infty} \frac{d\gamma}{2\pi i} e^{\bar{\alpha}_S \chi(\gamma)(Y-Y_0)+(\gamma-1)\xi} n_{\text{in}}(\gamma)$$

(18)

where $\chi(\gamma)$ is given by Eq. (9) and $\xi = \ln(1/(r^2 Q_s^2(Y_0)))$ with $r \equiv x_{01}$. In the definition of ξ we introduce a new momentum scale which characterizes the value of the initial condition. For simplicity, we have that

$$N(Y = Y_0, r) = r^2 Q_s^2(Y_0).$$

(19)

We can view this momentum as the saturation momentum at $Y = Y_0$, since $N \sim 1$ at $r^2 = 1/Q_s^2(Y_0)$. Equation (19) leads to $n_{\text{in}} = \frac{1}{\gamma}$.

Finally,

$$\int d^2 b N(Y;\boldsymbol{x}_{01},\boldsymbol{b}) = \int_{\epsilon-i\infty}^{\epsilon+i\infty} \frac{d\gamma}{2\pi i} e^{\bar{\alpha}_S \chi(\gamma)(Y-Y_0)+(\gamma-1)\xi} \frac{1}{\gamma}$$
$$= \int_{\epsilon-i\infty}^{\epsilon+i\infty} \frac{d\gamma}{2\pi i} e^{\Psi(Y,\xi,\gamma)} \frac{1}{\gamma}$$

(20)

In the vicinity of the saturation scale, the integral over γ can be evaluated using the method of steepest descent, with the equations for the saddle point $\gamma_{SP} \equiv \gamma_{cr}$:

(1) $\bar{\alpha}_S \chi(\gamma_{cr})(Y - Y_0) + (\gamma_{cr} - 1)\xi = 0$;

$$(2) \ \bar{\alpha}_S \left.\frac{d\chi(\gamma)}{d\gamma}\right|_{\gamma=\gamma_{cr}} (Y - Y_0) + \xi = 0.$$

(21)

Dividing the first equation by the second one, we obtain the value for $\bar{\gamma} = 1 - \gamma_{cr}$ which is the solution of Eq. (8).

The first equation gives the value of the saturation momentum

$$\ln(Q_s^2(Y)/Q^2(Y_0)) = \bar{\alpha}_S \frac{\chi(\gamma_{cr})}{1-\gamma_{cr}}(Y - Y_0) = \lambda(Y - Y_0)$$

(22)

Expanding $\Psi(Y,\xi,\gamma)$ at $\gamma \to \bar{\gamma}$ we obtain

$$\Psi(Y,\xi,\gamma) = \bar{\gamma}z - (\gamma - \gamma_{cr})z + \frac{1}{2}\bar{\alpha}_S \left.\frac{d^2\chi(\gamma)}{d\gamma^2}\right|_{\gamma=\gamma_{cr}}$$
$$\times (\gamma - \gamma_{cr})^2(Y - Y_0)$$
$$\text{where } z = \ln \tau^2 = \lambda(Y - Y_0) - \xi$$

(23)

Plugging Eq. (23) into Eq. (20) and integrating over $\gamma - \gamma_{cr}$, the resulting solution can be written in the form

$$N(Y = \ln(1/x); r, b) = N_0(r^2 Q_s(Y,b))^{\gamma_{\text{eff}}} = N_0(\tau)^{2\gamma_{\text{eff}}}$$

(24)

with

$$\bar{\gamma} \to \gamma_{\text{eff}} = \bar{\gamma} + \frac{\ln(1/\tau)}{\kappa\lambda \ln(\frac{1}{x})} \quad \text{with}$$

$$\kappa = \left.\frac{\chi''_{\gamma\gamma}(\gamma)}{\chi'_\gamma(\gamma)}\right|_{\gamma=\gamma_{cr}} \approx 9.9 \text{ in LO BFKL.} \quad (25)$$

In the method of steepest descend, the saddle point for the integration turns out to be

$$(\gamma - \gamma_{cr})_{SP} = \frac{z}{\bar{\alpha}_S \left.\frac{d^2\chi(\gamma)}{d\gamma^2}\right|_{\gamma=\gamma_{cr}}(Y - Y_0)}$$

(26)

4. Impact-parameter dependent CGC dipole model

As we have mentioned, the advantage of Eq. (24) is that we can introduce the correct behavior of the amplitude at large impact parameter, by imposing the phenomenological decrease in saturation momentum for large b, by writing it in the form:

$$Q_s = Q_s(x)S(b) = Q_0\left(\frac{1}{x}\right)^\lambda S(b)$$

(27)

In the LO BFKL [1] $\lambda = \bar{\alpha}_S \frac{\chi(\gamma_{cr})}{\bar{\gamma}}$. Parameters N_0 and Q_0, as well as function $S(b)$ should in future be taken from

TABLE I. Fitted parameters of the model [26], which we use for our estimates.

$\bar{\gamma}$	N_0	λ	x_0	B_{CGC} (GeV^{-2})
0.6599 ± 0.0003	0.3358 ± 0.0004	0.2063 ± 0.0004	0.00105 ± 1.1310^{-5}	5.5

nonperturbative QCD calculations but, at the moment, has to be determined from a fit to experimental DIS data. We have two models [26,39][3] on the market that describe the final set of the HERA experimental data on deep inelastic structure functions [42]. They have different forms for $S(b)$:

$$\text{Ref.[15]:} \quad \rightarrow S(b) = \exp\left(-\frac{b^2}{B}\right) = \exp\left(-\frac{b^2}{4\bar{\gamma}B_{CGC}}\right);$$
$$(28)$$

$$\text{Ref.[41]:} \quad \rightarrow S(b) = (mbK_1(mb))^{1/\bar{\gamma}};$$
$$(29)$$

The ansatz of Eq. (29) is preferable, since it leads to $S(b) \overset{b \gg 1/m}{\rightarrow} \exp(-mb)$, which is in accord with the Froissart theorem [43]. However, we choose Eq. (28) which allows us to do several integrations analytically. Using Eq. (30), $\nabla_T^2 N$ takes the following form, after integrating over b:

$$\int d^2b \nabla_T^2 N(Y,r,b)$$
$$= \frac{1}{r^2} \begin{cases} 8\pi B\bar{\gamma}N_0\tau^{2\bar{\gamma}}(1-N_0\tau^{2\bar{\gamma}}); & \text{for } \tau = rQ_s(x) < 1 \\ 8\pi B\bar{\gamma}\phi_0\tau^{2\bar{\gamma}}\exp(-2\phi_0\tau^{2\bar{\gamma}}) & \text{for } \tau = rQ_s(x) > 1; \end{cases}$$
$$(30)$$

with $\phi_0 e^{-2\phi_0} = N_0(1-N_0)$.

Before discussing the details of our model, we would like to outline, which features of Eq. (30) stem from the theorem, and which from phenomenological assumptions. The expression for $\tau \leq 1$, as we have mentioned [see Eq. (7)] follows from the theory. However, the calculation of N_G [see Eq. (5)] takes into account the term of the order N^2. The corrections of the order of N^2 has to be estimated for $\tau < 1$ and, in principle, they change Eq. (7). In Ref. [2] we discussed these corrections, but we do not take them into account, in Eq. (30) as we view $N = N_0\tau^{2\bar{\gamma}}$ as a phenomenological expression that describes the DIS data [26].

The fact that the impact parameter behavior of the saturation momentum determines the b-dependence of the scattering amplitude, comes from theory, while the particular form and result of integration over b, stems from the model for $S(b)$.

For $\tau \geq 1$ we have discussed the form of Eq. (30) in the previous section (see also Ref. [2]). The b integration is performed with the phenomenological $S(b)$.

In our estimates we use the values of the parameters from Ref. [26] (see Table I). In this paper the HERA data were fitted in the wide range of Q^2 from 0.75 GeV^2 to 650 GeV^2. The expression for $Q_s(x)$ in this model is taken in the form[4]

$$Q_s(x) = \frac{1}{2}\left(\frac{x_0}{x}\right)^{\frac{\lambda}{2}} \text{ GeV}$$
$$(31)$$

It should be noted, that the value of x from Eq. (13) even at $W = 13$ TeV, is about 10^{-5}, which is in the region that has been measured at HERA.

5. Inclusive production for $p_T \gg Q_s$

We can significantly simplify our calculation for $p_T \gg Q_s$. Indeed, for such large p_T the integral over r in Eq. (4) is concentrated in the region $\tau \ll 1$, where we can safely use the simple expression of Eq. (14). The integral can be calculated explicitly and leads to the following

$$\frac{d\sigma_G}{dyd^2p_T} = \frac{2C_F}{\alpha_s 2\pi}\frac{1}{p_T^2}N_0^2B^2\bar{\gamma}^2\left(\frac{\Gamma(2\bar{\gamma}-1)}{\Gamma(2-2\bar{\gamma})}(\tilde{p}_T)^{2-4\gamma_{\text{eff}}}\right.$$
$$- N_0 2^{2\bar{\gamma}+1}\frac{\Gamma(3\bar{\gamma}-1)}{\Gamma(2-3\bar{\gamma})}(\tilde{p}_T)^{2-6\gamma_{\text{eff}}}$$
$$\left.+ N_0^2 2^{2\bar{\gamma}}\frac{\Gamma(4\bar{\gamma}-1)}{\Gamma(2-4\bar{\gamma})}(\tilde{p}_T)^{2-8\gamma_{\text{eff}}}\right)$$
$$(32)$$

We know that in the vicinity of the saturation scale the scattering amplitude in the momentum representation has the following behavior:

$$N(p_T) = \text{Const}\left(\frac{p_T^2}{Q_s^2(x)}\right)^{\bar{\gamma}}$$
$$(33)$$

Therefore, from Eq. (32) we can determine the value of the constant in Eq. (33) from the value of N_0.

Equation (32) allows us to take into account the violation of the geometric scaling behavior, given by Eqs. (24) and (25). We can make such a replacement directly in the momentum representation, since $r \propto 1/p_T$. However, we

---

[3]Actually, the same set of the data was described in the model of Ref. [40], but this model does not include the correct behavior deep in the saturation region[41], and we do not discuss it here.

[4]Note that we introduce the extra factor $\frac{1}{2}$ in the definition of the saturation scale, since we use $\tau = rQ_s$, while in Ref. [26] τ is defined as $\tau = rQ_s/2$.
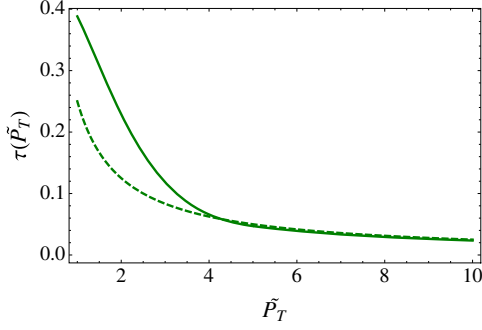
FIG. 1. The average τ [see Eq. (34)]. The solid line is the result of numerical calculations. The dotted line shows that at large $\tilde{p}_T$ $\langle\tau\rangle \propto 1/(4\tilde{p}_T)$. The figure is taken from Ref. [2]. $\tilde{p}_T = p_T/Q_s$.

need to find the coefficient in front of p_T and, perhaps, an additional constant. We calculate the average τ using the expression:

$$\langle\tau\rangle(\tilde{p}_T) = \frac{\int \tau J_0(\tilde{p}_T\tau)I(\tau)d\tau}{\int J_0(\tilde{p}_T\tau)I(\tau)d\tau} \quad \text{where}$$

$$I(\tau) = \int d^2b S(b)\left(\frac{d^2N_G(z(r,b,x_1)))}{dz^2}\right)^2 \quad (34)$$

The results of these estimates are shown in Fig. 1. One can see at $\tilde{p}_T \to 0 \langle\tau\rangle = 0.478 \approx \frac{1}{2}$ while at large $\tilde{p}_T$ it is proportional to $1/(4\tilde{p}_T)$.

For $\tilde{p}_T = 0$, or more generally for $p_T \ll Q_s$, the typical distance turns out to be $r = 1/(2Q_s(x))$, and for large $\tilde{p}_T$ it is of the order of $1/(4p_T)$. Hence, we suggest to use in Eq. (25) the calculated $\langle\tau\rangle(\tilde{p}_T)$ for $\tilde{p} \leq 4$ and $1/(4\tilde{p}_T)$ for $\tau \geq 4$ and to substitute in Eq. (32):

$$\gamma_{\text{eff}}(\tilde{p}_T, x) = \bar{\gamma} + \frac{\ln(1/\langle\tau\rangle(\tilde{p}_T))}{\kappa\lambda\ln(\frac{1}{x})} \quad (35)$$

where $\tilde{p}_T = p_T/Q_s$.

In Ref. [2] it was shown that this replacement results in the $\gamma_{\text{eff}} > 1$ at large $\tilde{p}_T$. This dependence is essential for

describing the experimental data. Indeed, the value of n in the hard term in Eq. (2) is $n = 3.1$. As we have seen above [see Eq. (32) for example] at large p_T the inclusive cross section is proportional to $1/p_T^{4\gamma_{\text{eff}}}$. For $\gamma_{\text{eff}} = \bar{\gamma}$ it is impossible to obtain a decrease of about $1/p_T^6$, as indicated by the data, while Eq. (35) makes such a description possible (see Ref. [2] for a detailed discussion).

C. Dipole-nucleus scattering amplitude

For the dipole-nucleus scattering amplitude in the vicinity of the saturation scale $\tau \sim 1$ we have the same behavior as for the dipole-nucleon amplitude:

$$N^A(Y, r, b) = \text{Const}(r^2Q_S(A, Y, b))^{\bar{\gamma}}. \quad (36)$$

The main question that we will try to answer in this section is how the value of Const in Eq. (36) is related to N_0 for the dipole-nucleon scattering amplitude.

The principle difference between scattering with a nucleus and a nucleon is shown in Fig. 2. For dipole-nucleon scattering the initial condition at $Y = Y_0 \equiv Y_{\text{min}}$ is such that $N(Y = Y_0, r, b) \ll 1$ [see Fig. 2(a)]. On the other hand, for dipole-nucleus scattering even at $Y = Y_0$ the shadowing corrections are large, and we impose the initial conditions inside the saturation region [see Fig. 2(b)]. These initial conditions lead to different solutions for dipole-hadron and dipole-nucleus amplitude in the saturation region (see Refs. [44–47]). In particular, for $\xi < 0$, where we expect geometric scaling behavior of the scattering amplitude, and for $\xi > 0$ and no such behavior is seen. However, a glance at Fig. 2, shows that for $Y - Y_{\text{min}} \gg 1$ for $\nabla_T^2 N^A(Y, r, b)$ we do not expect violation of the geometric scaling behavior of the scattering amplitude, since, as has been discussed in the previous section, this observable gives the main contribution in the vicinity of the saturation scale shown by the red line in Fig. 2. As we have discussed for the case of the dipole-nucleon scattering, the behavior of the scattering amplitude in the vicinity of the
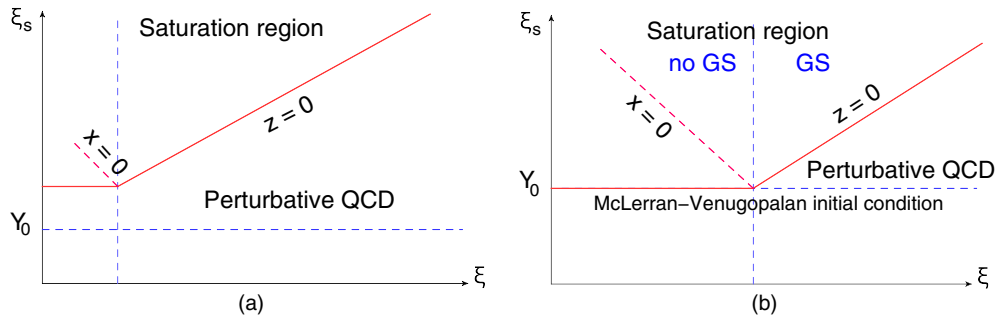

FIG. 2. The QCD map. Figure 2(a) shows the kinematic regions for the dipole-nucleon amplitude, while in Fig. 2(b), we show the kinematic regions for dipole-nucleus scattering. Note that the saturation domain in this case can be divided in two subregions: (i) for $\xi < 0$, where we expect geometric scaling behavior of the scattering amplitude, and $\xi > 0$ where there is no such behavior. $\xi_s = \lambda(Y - Y_{\text{min}})$ and $\xi = -\ln(\tau^2) = \ln(r^2Q_s^2)$. $z = \xi_s - \xi$ and $x = \xi + \xi$.
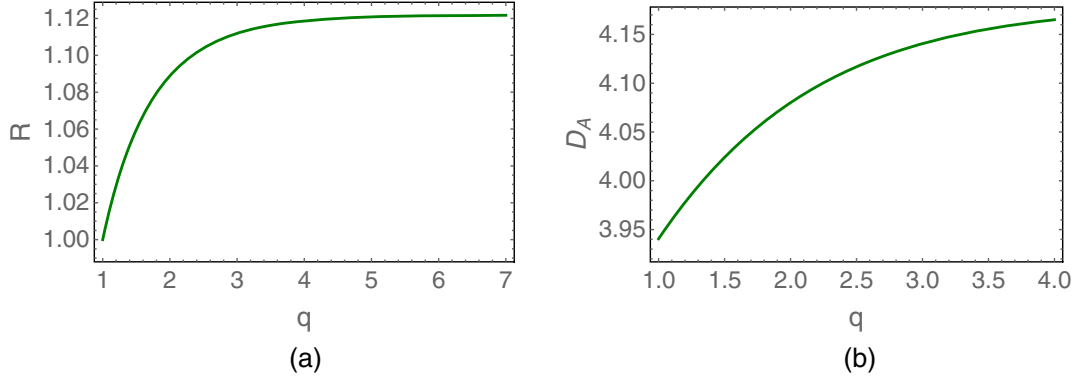
FIG. 3.   Figure 3(a): R vs $q = Q_s^2(A, Y_0, b)/Q_s^2(Y_0)$ (see Eq. (41)). Figure 3(b): D_A as function of q.

saturation scale is determined by the solution to the linear BFKL equation [see Eq. (16)].

Therefore, to find the value of Const in Eq. (36), we need to solve the BFKL equation with the correct initial condition. This condition is given by the McLerran-Venugopalan formula [5], which we use in the simplified form;

$$N_{in}^A(Y = Y_0; r, b) = 1 - \exp(-r^2 Q_s^2(A, Y = Y_0, b)). \quad (37)$$

The general solution to the BFKL equation of Eq. (16) has the same form as in Eq. (18):

$$N^A(Y; \boldsymbol{x}_{01}, \boldsymbol{b}) = \int_{\epsilon - i\infty}^{\epsilon + i\infty} \frac{d\gamma}{2\pi i} e^{\bar{\alpha}_S \chi(\gamma)(Y - Y_0) + (\gamma - 1)\xi}$$
$$\times n_{in}\left(\gamma, \frac{Q_s^2(A, b)}{Q_s^2(Y_0)}\right) \quad (38)$$

where $Q_s(Y_0)$ has been introduced in Eq. (19). We recall that $\xi = -\ln(r^2 Q_s^2(Y_0))$. Using Eq. (37) we can find $n_{in}^A(\gamma, \frac{Q_s^2(A, Y_0, b)}{Q_s^2(Y_0)})$ we takes the following form:

$$n_{in}^A\left(\gamma, \frac{Q_s^2(A, Y_0, b)}{Q_s^2(Y_0)}\right)$$
$$= \left(\frac{Q_s^2(A, Y_0, b)}{Q_s^2(Y_0)}\right)^{1-\gamma} \left(\Gamma(\gamma) - \Gamma\left(\gamma, \frac{Q_s^2(A, Y_0, b)}{Q_s^2(Y_0)}\right)\right). \quad (39)$$

Plugging Eq. (39) into Eq. (38) we obtain the following solution:

$$N^A(Y; \boldsymbol{x}_{01}, \boldsymbol{b}) = \int_{\epsilon - i\infty}^{\epsilon + i\infty} \frac{d\gamma}{2\pi i} e^{\bar{\alpha}_S \chi(\gamma)(Y - Y_0) + (\gamma - 1)\xi_A}$$
$$\times \left(\Gamma(\gamma) - \Gamma\left(\gamma, \frac{Q_s^2(A, Y_0, b)}{Q_s^2(Y_0)}\right)\right) \quad (40)$$

where $\xi_A = -\ln(r^2 Q_s^2(A, Y_0, b))$.

Solving Eq. (21), we obtain the solution in the vicinity of saturation, in the form of Eq. (36) scale with

$$\text{Const} = N_0 \frac{\left(\Gamma(\gamma_{cr}) - \Gamma\left(\gamma_{cr}, \frac{Q_s^2(A, Y_0, b)}{Q_s^2(Y_0)}\right)\right)}{(\Gamma(\gamma_{cr}) - \Gamma(\gamma_{cr}, 1))} = N_0 R \quad (41)$$

In Fig. 3 we plot the value of R as function of $q = Q_s^2(A, Y_0, b)/Q_s^2(Y_0)$. One can see that R is very close to 1. The chosen range of q we will be discussed in the next section. In further estimates, we take Const $= N_0$.

As we discussed in the previous section, Eq. (35) which takes into account the violation of the geometric scaling behavior, is essential for the description of the experimental data, since the region of perturbative QCD gives a large contribution. Bearing this in mind, we take into account the contribution of $n_{in}^A(\gamma, \frac{Q_s^2(A, Y_0, b)}{Q_s^2(Y_0)})$ into effective γ_{eff} as well as Eq. (35). Considering the resulting Ψ in Eq. (20) in the form

$$\Psi(Y, \xi_A, \gamma) = \bar{\alpha}_S \chi(\gamma)(Y - Y_0) + (\gamma - 1)\xi$$
$$+ \ln\left(n_{in}^A\left(\gamma, \frac{Q_s^2(A, Y_0, b)}{Q_s^2(Y_0)}\right)\right) \quad (42)$$

we obtain the following expression for the effective γ:

$$\gamma_{eff} = \bar{\gamma} + \frac{\ln(1/\tau)}{\kappa\lambda \ln(\frac{1}{x})} + 2D_A \frac{\ln(1/\tau)}{(\kappa\lambda \ln(\frac{1}{x}))^2} \quad (43)$$

where κ is defined in Eq. (35). Recall that $\tau = rQ_s(A, Y)$. The value of D_A is plotted in Fig. 3(b), as a function of $q = Q_s^2(A, Y_0, b)/Q_s^2(Y_0)$. In the region of $q = 1.5$–4 $D_A \approx 4$, and we will argue below that this region contributes to the ion-ion collisions at the LHC energies.

III. KLN MODEL FOR ION-ION SCATTERING AT HIGH ENERGY

Figure 4 shows the interaction of two nucleus A_1 and A_2. From this picture we see that we need to know how many nucleons interact, and how this interaction occurs. In particular, one nucleon can interact with several nucleons from another nucleus, and so on. We use the KLN model to answer all similar questions (see Refs. [25,37,48–52]).
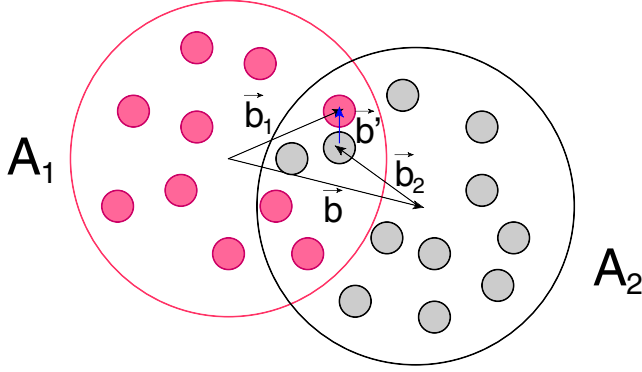
FIG. 4. The kinematics for the nucleus-nucleus interaction. $\boldsymbol{b}_1$ denotes the position of the nucleon in the transverse plane in the nucleus A_1. $\boldsymbol{b}_2$ the position of the nucleon in nucleus A_2. b denotes the distance between the centers of two nuclei $\boldsymbol{b} = \boldsymbol{b}_1 - \boldsymbol{b}_2$. The two nucleons from different nuclei, which interact at distance $\boldsymbol{b}'$, are shown by different colors in the figure.

We choose this model since, on one hand, this model not only successfully described the RHIC data and its predictions for the experimental data at the LHC, are quite good. On the other hand, it is based on the Glauber approach [53,54], which successfully describes the nucleus-nucleus interaction over a wide energy range. In Refs. [49,55] the Glauber approach is developed for the hadron production for nucleus-nucleus collisions, and it demonstrates how we can calculate (i) the number of nucleons that participate in the interactions (number of participants N_{part}), their density ρ_{part} at fixed values of b; and (2) how to correlate the typical values of b with the centrality c, which is measured experimentally, and which characterizes the percentile of events with the largest number of produced particles (as registered in detectors). Experimentally collisions are grouped into event(centrality) classes, with the most central class defined by events with the highest multiplicity(smallest forward energy), which corresponds to small values of the impact parameter. Basically centrality $c(N)$ is equal to

$$c(N) \simeq \frac{\pi b(N)}{\sigma_n}, \qquad (44)$$

where $c(N)$ is the centrality of the events with the multiplicity higher than N. $b(N)$ is the value of the impact parameter for which the average multiplicity $n(b(N)) = N$.

In our approach, we use the estimates of Ref. [49] for the density of the participants at for different centrality classes.[5]

The key idea of the KLN model [37,49] is, that the saturation momentum is proportional to the density of the

---

[5]For comparison with the ALICE experimental data we use the results of the estimates, given by Ref. [56], in which the procedure of Ref. [49] is used in the Glauber Monte Carlo.

participants, $Q_s \propto \rho_{\text{part}}$. The arguments for this stem from the simple equation for the saturation momentum [1,3–5]

$$Q_s^2(A, Y) = \frac{8\pi^2 N_c}{N_c^2 - 1} \alpha_S(Q_s^2) \frac{xG_A(Q_s^2(A, Y), Y)}{\pi R_A^2} \qquad (45)$$

where $Y = \ln(1/x)$, N_c denotes the number of colors, R_A the radius of the nucleus and xG_A is the gluon structure function of the nucleus.

For the kinematic region where the gluon densities are small we can safely consider $G_A(Q^2, x) = AxG_N(Q^2, x)$, where G_N is the gluon structure function for a nucleon. Plugging this relation in Eq. (45) as well as $R_A = R_N A^{1/3}$, where R_N is the radius of the nucleon, we obtain that

$$Q_s^2(A, Y) = \frac{8\pi^2 N_c}{N_c^2 - 1} \alpha_S(Q_s^2) \frac{A}{\pi R_A} xG_N(Q_s^2(A, Y), Y)$$

$$= \rho_A \frac{8\pi^2 N_c}{N_c^2 - 1} \alpha_S(Q_s^2) xG_N(Q_s^2(A, Y), Y) \qquad (46)$$

where ρ_A is the density of the nucleons in the nucleus in the transverse plane.

The KLN model generalizes Eq. (46) proposing

$$Q_s^2(N_{\text{part}}, Y) = \frac{1}{2} \rho_{\text{part}} \frac{8\pi^2 N_c}{N_c^2 - 1} \alpha_S(Q_s^2) xG_N(Q_s^2(N_{\text{part}}, Y), Y). \qquad (47)$$

We suggest to rewrite Eq. (47) in the form

$$Q_s^2(N_{\text{part}}, Y)$$

$$= \frac{1}{2} \rho_{\text{part}} \pi R_N^2 \boxed{\frac{8\pi^2 N_c}{N_c^2 - 1} \alpha_S(Q_s^2) \frac{xG_N(Q_s^2(N_{\text{part}}, Y), Y)}{\pi R_N^2}}$$

$$= \frac{1}{2} \rho_{\text{part}} \int d^2 b Q_s^2(N, Y, b). \qquad (48)$$

Factor $\frac{1}{2}$ reflects the fact that we are dealing with the density of those nucleons in a single nucleus, which will participate in the collision at a given impact parameter b, or in a definite centrality class. In Eq. (48) we write the expression for the nucleon saturation momentum in the frame.

One can see that for the DIS with a nucleus with $N_{\text{part}} = A$ we obtain from Eq. (48)

$$Q_s^2(A, Y) = A^{1/3} Q_s^2(N, Y) \qquad (49)$$

in accord with Refs. [57–60]. Using the estimates of ρ_{part} from Ref. [49] we obtain that the range of q in Fig. 3 for the lead-lead scattering is $q = 1$–3.06.

For the gluon transverse momenta p_T distributions, we suggest the following formula for the ion-ion collisions in the definite centrality class with the number of participants N_{part}:

$$\frac{dn_G}{dy d^2 p_T}\bigg|_{N_{\text{part}}} = \frac{1}{2} N_{\text{part}} \frac{dN}{dy d^2 p_T}\bigg|_{\text{proton-proton}}$$

$$= \frac{1}{2} N_{\text{part}} \frac{1}{\sigma_{\text{in}}} \frac{d\sigma_G^N}{dy d^2 p_T}$$

$$= \frac{1}{2} N_{\text{part}} \frac{1}{\sigma_{\text{in}}} \frac{2C_F}{\alpha_s (2\pi)^4} \frac{1}{p_T^2} \int d^2 r e^{i p_T \cdot r}$$

$$\times \int d^2 b \nabla_T^2 N_G(y_1 = \ln(1/x_1); r, b)$$

$$\times \int d^2 b' \nabla_T^2 N_G(y_2 = \ln(1/x_2); r, b'), \quad (50)$$

where N_G is related to the scattering dipole-nucleon amplitude [see Eq. (5)], and n_G denotes the multiplicity of the emitted gluons.

σ_{in} denotes the inelastic cross section for the nucleon-nucleon scattering at corresponding energy. One can see, that in Eq. (50) we consider each participant as a nucleon which interacts with another nucleon from the different nucleus, at impact parameter b' (see Fig. 4). The saturation momentum for this scattering is given by Eq. (48), for the effective γ_{eff} we take Eq. (43), which includes corrections from the interaction with the other nucleons. We need also to fix the dependence of the saturation scale on the impact parameter of the nucleon-nucleon interaction (b' in Fig. 4). Finally, the equation for the saturation scale, which we use in our estimates of gluon production in nucleon-nucleon scattering, takes the form:

$$Q_s^2(N_{\text{part}}, Y, b') = \frac{1}{2} \rho_{\text{part}} \int d^2 b Q_s^2(Y, b) S(b') \quad (51)$$

where Q_s and $S(b')$ are given by Eqs. (27) and (28), respectively.

At first sight, we do not need Eq. (50), since we can use the master equation [see Eq. (4)] and using the experimental information of gluon structure functions of nucleus (see for example Ref. [61]), we can calculate the inclusive cross section as we did for proton-proton scattering in Ref. [2]. Indeed, for the inclusive production of gluons for an ion-ion collision, we can proceed in this manner, but the factorization of Eq. (4) is proven only in the case, when we did not make any additional selections of the events summing over all accompanying hadrons. Considering the different centrality classes we make the additional selection on the multiplicity of produced hadrons. It is sufficient to refer to the AGK cutting rules [62], to see that these selections violate the factorization of Eq. (4). The violation of the AGK cutting rules in QCD (see Ref. [1]) makes the situation even worse. Hence, the KLN model gives us the simple way to estimate the cross sections for the different centrality classes.

IV. COMPARISON WITH THE EXPERIMENT

We calculate the cross section for gluon production using Eq. (50). As we have discussed in Sec. II B, the typical values of r that contribute to the integral in Eq. (50) are rather small, of the order of Q_s. This means that we can safely use the CGC/saturation approach or/and the perturbative QCD estimates for this integral. We do not need to incorporate modifications of the gluon propagators, for example due to the confinement [34,35], in our calculations.

The factor $1/p_T^2$ in front in Eq. (50) stems from the gluon propagator [32], and it is affected both by the hadronization, and by interactions with comovers in the parton cascade. In our approach to the confinement problem, we first need to take into account, the effect of the mass of produced gluon jet due to hadronization, which changes the gluon propagator [37]:

$$G(p_T) = \frac{1}{p_T^2} \rightarrow \frac{1}{p_T^2 + 2(Q_s \Theta(Q_s - p_T) + p_T \Theta(p_T - Q_s)) m_{\text{eff}}}.$$
$$(52)$$

Therefore, we calculate gluon production using Eq. (50), in which we use Eq. (52) to replace the factor $1/p_T^2$. Therefore, our model of the hadronization consists of two ingredients: the decay of the gluon into hadron jet with the fragmentation function [see Eq. (11)], and to account for the mass of this jet, using Eq. (52). It is instructive to note, that in our approach we see two stages of the multiparticle production in an explicit way: the creation of the color glass condensate [calculation of the integral over r in Eq. (50)] and the stage of hadronization [Eq. (52), and fragmentation functions].

For calculating the integral over r in Eq. (50) we use Eq. (30) for $p_T \leq 2Q_s(x)$ and Eq. (32) for larger values of p_T (see Ref. [2] for more details). The values of σ_{in} for proton-proton scattering at high energies we take from Ref. [63], which describes all available data on measured soft cross sections.

We compare with the experimental data of ALICE collaboration [64–67] on the transverse momentum distribution of the charged hadrons in different centrality classes at two energies $W = 5$ TeV and $W = 2.78$ TeV. We add to Eq. (50) the thermal term[6] [see first term of Eq. (2)], and find that in our model of hadronization we need this term to describe the experimental data. The value of this contribution essentially depends on the mass of the gluon jet in the framework of our model. It turns out that the temperature T_{th} is proportional to the value of the saturation scale in the given centrality class in accord with Eq. (1), but the coefficient c turns out to be 1.5 larger than it is predicted in Ref. [11] ($c = 1.8$).

---

[6]The value of the parameter A_{therm} is determined by comparison with the experimental data.
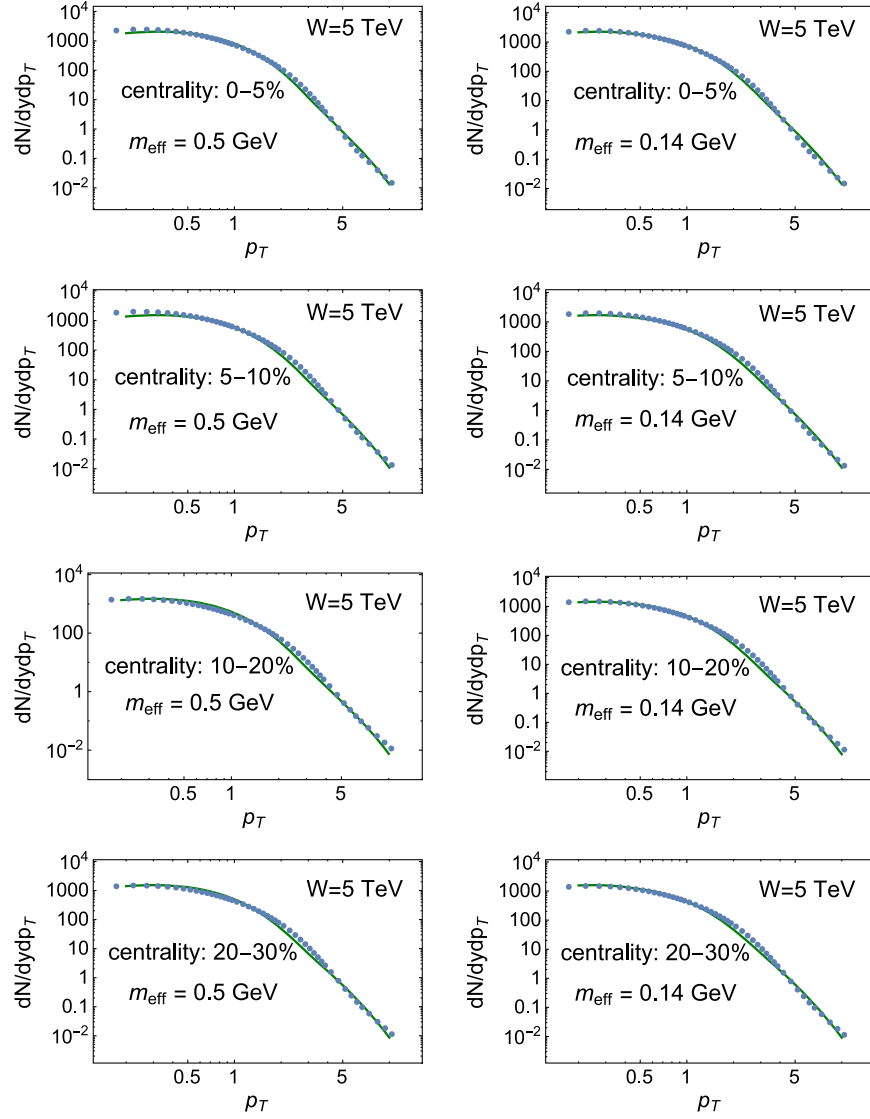
FIG. 5. Descriptions of the experimental data of the ALICE collaboration [66,67] for lead-lead collisions at $W = 5$ TeV for different centralities (solid lines). The dashed lines show the CGC contributions. For the value of σ_{in} in Eq. (50) at $W = 5$ TeV we use the model of Ref. [63], for $\sigma_{in} = \sigma_{tot} - \sigma_{el} - \sigma_{diff}$.

In Figs. 5–7 we show that we describe the data fairly well in the region $p_T \leq 10$ GeV. It should be noted that we do not need any K-factor which would account for the higher order corrections in the framework of CGC/saturation approach.

However, this conclusion we need to take with a degree of skepticism, since the value of σ_{in} was taken from the model [63], and the value of $\bar{\alpha}_S$ in Eq. (50) was taken $\bar{\alpha}_S = 0.25$. The main uncertainty in $\sigma_{in} = \sigma_{tot} - \sigma_{el} - \sigma_{diff}$ is the value of σ_{diff}, which at high energies is about 15%–20% of the total cross sections. The value of $\bar{\alpha}_S(Q_s^2) \approx 0.3$–$0.4$. Therefore, these two uncertainties can lead to the $K \approx 2$.

Figures 5–7 show that we describe the behavior of the transverse momentum distribution at $p_T \geq 2$ by Eq. (50),

rather well. We wish to note that this description stems from the expression for γ_{eff} [see Eq. (43)], in which the last term comes from the corrections related to the nucleus target. In the description of p_T distribution, these corrections are considerable.

The rate of thermal radiation is shown in Table II, in which $R = \int d^2 p_T d^2 \sigma_{therm\,rad}^{charged}/d^2 p_T / \int d^2 p_T d^2 \sigma_{sum}^{charged}/d^2 p_T$. Note that the contribution of the thermal radiation increases with the growth of energy. The value of the CGC term depends on the value of the m_{eff}. We believe that most of the pions are produced from ρ resonances and we consider $m_{eff} = 0.5$ GeV. We recall that the simple formula for $m_{eff} = \sqrt{\mu^2 + k_T^2 + k_L^2} - k_L$ leads to $m_{eff} = 0.5$ GeV if μ is equal to the mass of ρ-resonance since the value of
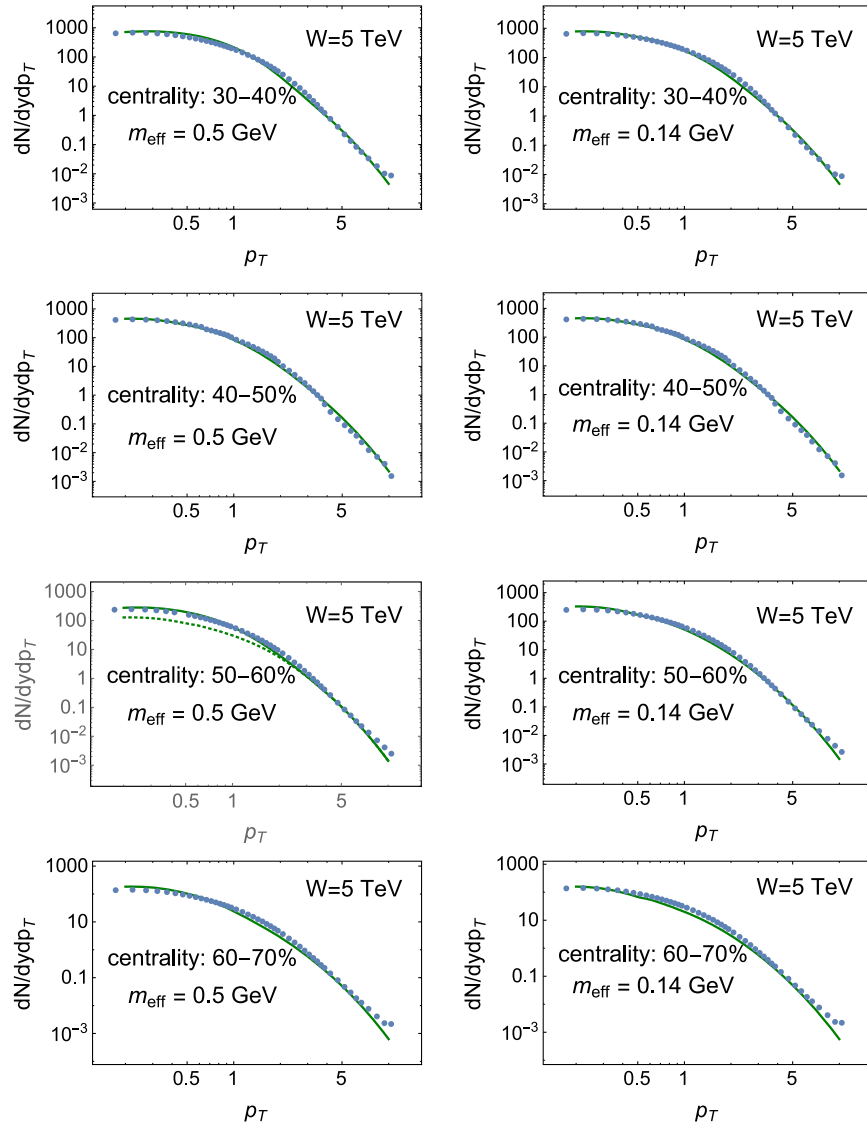
FIG. 6. The continuation of Fig. 5.

$k_T = k_L = 0.45$ GeV (see Ref. [68] for the measurement and Ref. [69]) and reference therein for theoretical discussions). For the minimal mass of $\mu = m_\pi = 0.14$ GeV we obtain $m_{\text{eff}} = 0.2$ GeV. To illustrate the influence of the mass of gluon jet we estimate the contribution of Eq. (50) with $m_{\text{eff}} = 0.14$ MeV. One can see that even such small mass cannot describe the spectrum without the thermal radiation term. We see from Figs. 5–7, and Table II that the value of this term depends on the value of m_{eff}.

In Fig. 8 we plot the estimates for the p_T distribution with $m_{\text{eff}} = 0$. In this case we have the divergence $G(p_T) \propto 1/p_T^2$, We have not ignored this divergence, and have plotted $p_T \geq 200$ MeV. It turns out that we need to add the thermal emission with R = 42%. This should be compared with the proton-proton scattering [2], where for $m_{\text{eff}} = 0$ we do not need to add the thermal emission.

In general, comparing Table II with the estimates for the ratio R for proton-proton scattering (see Table II of Ref. [2]) we see that the contributions of the thermal radiation are larger for ion-ion collisions for the classes with small centrality. It supports the CGC picture in which the longitudinal fields, that are the sources of the thermal radiation, are stronger in the denser gluon states which are produced in ion-ion collisions.

Discussing hadron production, we have to construct a model for the process of hadronization. Our model where the production of the gluon jets with the hadronization, which is given by the fragmentation functions and by the mass of the gluon jet, requires a thermal radiation term. Our estimates for $m_{\text{eff}} = 0$ show that, possibly, our claim does
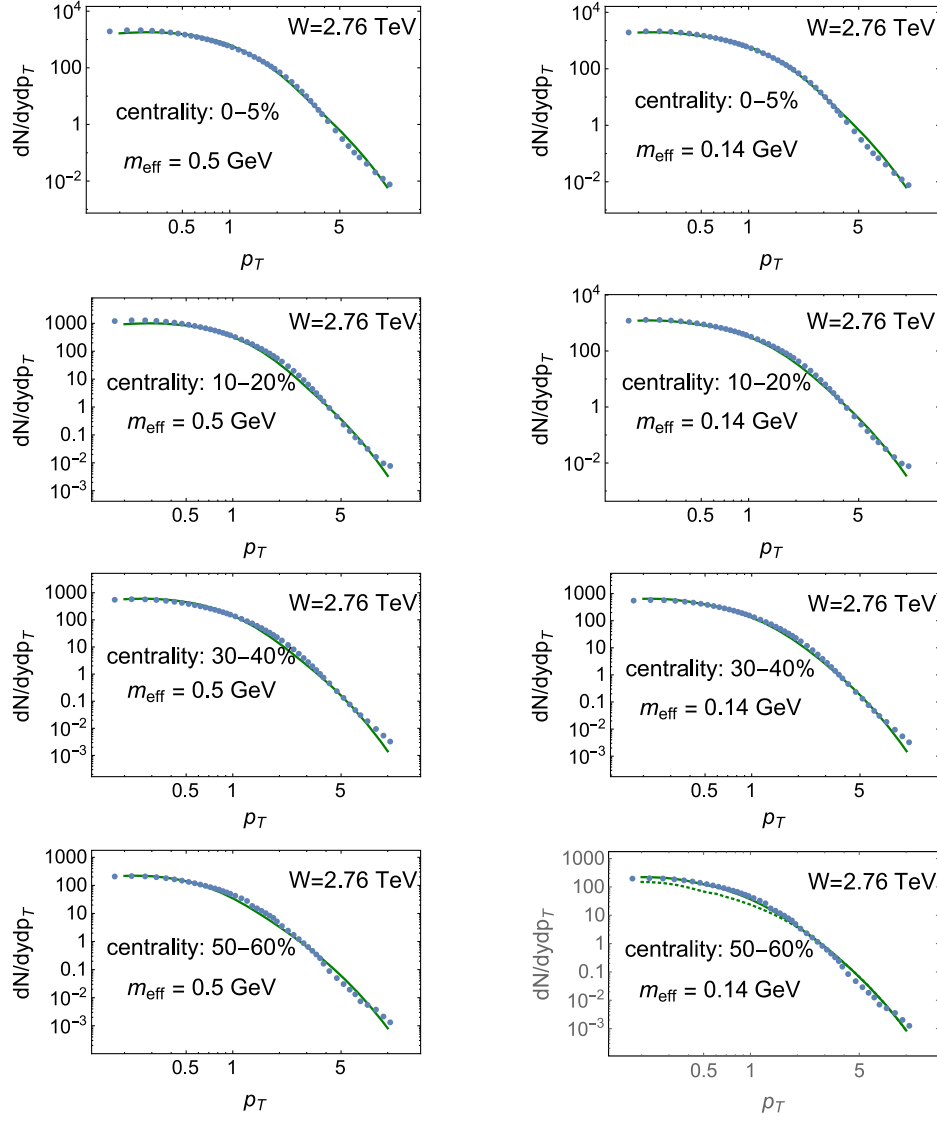
FIG. 7. The descriptions of the experimental data of the ALICE collaboration [65–67] for lead-lead collisions at $W = 2.76$ TeV for different centralities (solid lines). The dashed lines show the CGC contributions. For the value of σ_{in} in Eq. (50) at $W = 2.76$ TeV we use the model of Ref. [63], for $\sigma_{in} = \sigma_{tot} - \sigma_{el} - \sigma_{diff}$.

TABLE II. $R = d^2\sigma^{charged}/d^2 p_T(\text{thermal radiation})/d^2\sigma^{charged}/d^2 p_T(\text{sum})$ for different the centrality classes vs the values of m_{eff}.

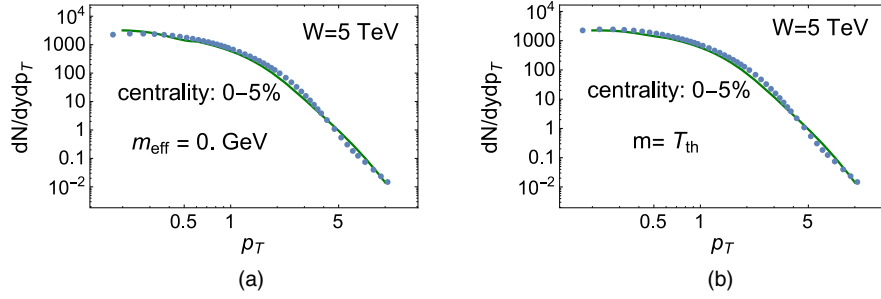| Centrality | W = 5 TeV | | W = 2.76 TeV | |
	$m_{eff} = 0.5$ GeV	$m_{eff} = 0.14$ GeV	$m_{eff} = 0.5$ GeV	$m_{eff} = 0.14$ GeV
0%–5%	76%	63%	66%	52%
5%–10%	72%	58%		
10%–20%	72%	58%	52%	43%
20% −30%	72%	54%		
30%–40%	62%	37%	62%	34%
40%–50%	60%	37%		
50%–60%	51%	20%	60%	12%
60%–70%	43%	13%		

FIG. 8.   Descriptions of the experimental data of the ALICE collaboration [66,67] for lead-lead collisions at $W = 5$ TeV for centrality 0–5% with $m_{eff} = 0$ [Fig. 8(a)] and with $m = T_{th}$ for the gluon propagator $1/(p_T^2 + m^2)$ [Fig. 8(b)]. In both figures $R \approx 46\%$.

not depend on the model of the hadronization in the case of the ion-ion collisions, since the description of the experimental data in Fig. 8(a) requires a thermal radiation term of the order of 46%. In Fig. 8(b) we plot the p_T spectrum for a different model, with the gluon propagator $1/(p_T^2 + m^2)$ with $m = T_{th}$, instead of Eq. (52). It turns out that R = 46% is needed to describe the data. The last case corresponds to a different hadronization model: the propagator of the gluon with transverse momentum p_T in the CGC medium with the temperature T_{th}, acquires a mass $m_g \propto T_{th}$ [70] and the propagator has the form $1/(p_T^2 + m_g^2)$. This mass provides the infrared cutoff in the gluon spectrum. However, we need to take our estimates in Fig. 8(b) with a grain of salt, since Ref. [70] predicts that the gluon mass will be $m = gT$ but with small value of g. However, Fig. 8(a) supports our claim, that the requirement of the thermal emission does not depend on the details of the assumption on the confinement of quarks and gluon.

V. CONCLUSIONS

The main result of the paper is that we show that a thermal emission term is required to describe the transverse momenta distribution for charged particles in ion-ion collision. The temperature of this emission T_{th} turns out to proportional to the saturation scale [see Eq. (1)] with coefficient $c = 1.8$, which is 1.5 times larger than predicted in Ref. [11].

We develop the formalism for the calculation of the transverse momenta spectra in CGC/saturation approach, in which we clearly see two stages of the process: the creation of color glass condensate, and the hadronization stage. Our calculations are based on the observation that even for small values of p_T the main contribution in the integration over r in Eq. (4) and in Eq. (50) stems from the kinematic region in the vicinity of the saturation momentum, where theoretically, we know the scattering amplitude. In other words, it means that we do not need to introduce the nonperturbative corrections due to the unknown physics at long distances (see Refs. [34,35] for example) in the dipole

scattering amplitude. The nonperturbative corrections have to be included to describe the process of hadronization, which we discuss in the model. This model incorporates the decay of the gluon jet with the effective mass $m_{eff}^2 = 2Q_s\mu_{soft}$ where μ_{soft} is the soft scale, and with the fragmentation functions of Eq. (12), at all values of the transverse momenta.

It should be emphasized that we reproduce the experimental data without any K-factor, which is used for accounting of the higher order corrections. We wish to mention, that we have calculated the inclusive production taking $\bar{\alpha}_S = 0.25$. This value is less that $\bar{\alpha}_S(Q_s) = 0.3$–$0.4$ which appears more natural in Eq. (50). For $\bar{\alpha}_S = \bar{\alpha}_S(Q_s)$, we need to introduce a K-factor of about 1.3–1.6.

We use the KLN model [25,37,48–52] which gives us the simple way to estimate the cross sections for the different centrality classes. At first sight, we do not need Eq. (50), since we can use the master equation [see Eq. (4)], and using the experimental information of gluon structure functions of nucleus (see for example Ref. [61]) we can calculate the inclusive cross section, as we did for proton-proton scattering in Ref. [2]. However, considering the different centrality classes, we make the additional selection on the multiplicity of produced hadrons, which violates the factorization of Eq. (4). The KLN model suggests a way to evaluate the contribution of the different centrality classes.

Comparing the results of this paper with our discussion of the transverse distribution in the proton-proton scattering [2] we see two major differences. First, we need the larger contribution of the thermal radiation term, since we produce in the ion-ion collision the CGC with higher parton densities. Second, changing the model for the hadronization, we failed to describe the p_T spectrum without the thermal radiation term. In Fig. 8 we illustrate this fact showing that the divergence, coming from the factor $1/p_T^2$ in Eq. (50), does not lead to a sufficiently large contribution that we could describe the data without the thermal radiation term, as was the case for hadron-hadron scattering [2]. Therefore, we suspect that the existence of the thermal radiation term does not depend on the model of confinement.

It should be mentioned that we include nuclei in the framework of the simple KLN model, neglecting a dynamical evolution of produced matter. We believe this is the correct first approximation in the CGC approach, in which we only took into account the dependence on the density of the matter, through the saturation scale. The result of our description can be interpreted as an argument that the production in nucleus-nucleus collision is very similar to the proton-proton scattering which has been discussed in our first paper.

[1] Y. V. Kovchegov and E. Levin, *Quantum Chromodynamics at High Energy* (Cambridge University Press, Cambridge, England, 2012), Vol. 33.

[2] E. Gotsman and E. Levin, Thermal radiation and inclusive production in the CGC/saturation approach at high energies, Eur. Phys. J. C **79**, 415 (2019).

[3] L. V. Gribov, E. M. Levin, and M. G. Ryskin, Semihard processes in QCD, Phys. Rep. **100**, 1 (1983).

[4] A. H. Mueller and J. Qiu, Gluon recombination and shadowing at small values of x, Nucl. Phys. **B268**, 427 (1986).

[5] L. McLerran and R. Venugopalan, Computing quark and gluon distribution functions for very large nuclei, Phys. Rev. D **49**, 2233 (1994); Gluon distribution functions for very large nuclei at small transverse momentum, Phys. Rev. D **49**, 3352 (1994); Green's function in the color field of a large nucleus, Phys. Rev. D **50**, 2225 (1994); Fock space distributions, structure functions, higher twists, and small x, Phys. Rev. D **59**, 094002 (1999).

[6] B. B. Abelev *et al.* (ALICE Collaboration), Energy dependence of the transverse momentum distributions of charged particles in pp collisions measured by ALICE, Eur. Phys. J. C **73**, 2662 (2013).

[7] R. Sassot, P. Zurita, and M. Stratmann, Inclusive hadron production in the CERN-LHC Era, Phys. Rev. D **82**, 074011 (2010).

[8] D. de Florian, R. Sassot, M. Epele, R. J. Hernández-Pinto, and M. Stratmann, Parton-to-pion fragmentation reloaded, Phys. Rev. D **91**, 014035 (2015).

[9] D. E. Kharzeev and E. M. Levin, Deep inelastic scattering as a probe of entanglement, Phys. Rev. D **95**, 114008 (2017).

[10] D. Kharzeev and K. Tuchin, From color glass condensate to quark gluon plasma through the event horizon, Nucl. Phys. **A753**, 316 (2005).

[11] D. Kharzeev, E. Levin, and K. Tuchin, Multi-particle production and thermalization in high-energy QCD, Phys. Rev. C **75**, 044903 (2007).

[12] O. K. Baker and D. E. Kharzeev, Thermal radiation and entanglement in proton-proton collisions at energies available at the CERN Large Hadron Collider, Phys. Rev. D **98**, 054007 (2018).

[13] G. V. Dunne and T. Hall, On the QED effective action in time dependent electric backgrounds, Phys. Rev. D **58**, 105022 (1998).

[14] P. Castorina, D. Kharzeev, and H. Satz, Thermal hadronization and hawking-unruh radiation in QCD, Eur. Phys. J. C **52**, 187 (2007).

[15] A. A. Bylinkin and A. A. Rostovtsev, Role of quarks in hadroproduction in high energy collisions, Nucl. Phys. **B888**, 65 (2014).

[16] A. A. Bylinkin and M. G. Ryskin, Secondary hadron distributions in two component model, Phys. Rev. D **90**, 017501 (2014).

[17] A. A. Bylinkin, D. E. Kharzeev, and A. A. Rostovtsev, The origin of thermal component in the transverse momentum spectra in high energy hadronic processes, Int. J. Mod. Phys. E **23**, 1450083 (2014).

[18] A. Bylinkin, N. S. Chernyavskaya, and A. A. Rostovtsev, Predictions on the transverse momentum spectra for charged particle production at LHC-energies from a two component model, Eur. Phys. J. C **75**, 166 (2015).

[19] X. Feal, C. Pajares, and R. A. Vazquez, Thermal behavior and entanglement in Pb-Pb and p-p collisions, Phys. Rev. C **99**, 015205 (2019).

[20] J. Adam *et al.* (ALICE Collaboration), Pseudorapidity and transverse-momentum distributions of charged particles in proton–proton collisions at $\sqrt{s} = 13$ TeV, Phys. Lett. B **753**, 319 (2016).

[21] M. Aaboud *et al.* (ATLAS Collaboration), Charged-particle distributions at low transverse momentum in $\sqrt{s} = 13$ TeV pp interactions measured with the ATLAS detector at the LHC, Eur. Phys. J. C **76**, 502 (2016).

[22] G. Aad *et al.* (ATLAS Collaboration), Charged-particle distributions in $\sqrt{s} = 13$ TeV pp interactions measured with the ATLAS detector at the LHC, Phys. Lett. B **758**, 67 (2016).

[23] V. Khachatryan *et al.* (CMS Collaboration), Transverse-Momentum and Pseudorapidity Distributions of Charged Hadrons in pp Collisions at $\sqrt{s} = 7$ TeV, Phys. Rev. Lett. **105**, 022002 (2010).

[24] A. M. Sirunyan *et al.* (CMS Collaboration), Measurement of charged pion, kaon, and proton production in proton-proton collisions at $\sqrt{s} = 13$ TeV, Phys. Rev. D **96**, 112003 (2017).

[25] A. Dumitru, D. E. Kharzeev, E. M. Levin, and Y. Nara, Gluon Saturation in pA Collisions at the LHC: KLN model predictions for hadron multiplicities, Phys. Rev. C **85**, 044920 (2012).

[26] A. H. Rezaeian and I. Schmidt, Impact-parameter dependent Color Glass Condensate dipole model and new combined HERA data, Phys. Rev. D **88**, 074016 (2013).

[27] Y. V. Kovchegov and K. Tuchin, Inclusive gluon production in DIS at high parton density, Phys. Rev. D **65**, 074026 (2002).

[28] J. Bartels and E. Levin, Solutions to the Gribov-Levin-Ryskin equation in the nonperturbative region, Nucl. Phys. **B387**, 617 (1992).

[29] A. M. Stasto, K. J. Golec-Biernat, and J. Kwiecinski, Geometric Scaling for the Total $\gamma^* p$ Cross-Section in the Low x Region, Phys. Rev. Lett. **86**, 596 (2001).

[30] E. Iancu, K. Itakura, and L. McLerran, Geometric scaling above the saturation scale, Nucl. Phys. **A708**, 327 (2002).

[31] A. H. Mueller and D. N. Triantafyllopoulos, The Energy dependence of the saturation momentum, Nucl. Phys. **B640**, 331 (2002).

[32] V. S. Fadin, E. A. Kuraev, and L. N. Lipatov, On the pomeranchuk singularity in asymptotically free theories, Phys. Lett. **60B**, 50 (1975); E. A. Kuraev, L. N. Lipatov, and V. S. Fadin, The pomeranchuk singularity in quantum chromodynamics, Zh. Eksp. Teor. Fiz. **72**, 377 (1977) [The pomeranchuk singularity in nonabelian gauge theoriesSov. Phys. JETP **45**, 199 (1977)]; I. I. Balitsky and L. N. Lipatov, The pomeranchuk singularity in quantum chromodynamics, Yad. Fiz. **28**, 1597 (1978) [Sov. J. Nucl. Phys. **28**, 822 (1978)].

[33] A. Kovner and U. A. Wiedemann, Nonlinear QCD evolution: Saturation without unitarization, Phys. Rev. D **66**, 051502, 034031 (2002); No Froissart bound from gluon saturation, Phys. Lett. B **551**, 311 (2003).

[34] N. Vandersickel and D. Zwanziger, The Gribov problem and QCD dynamics, Phys. Rep. **520**, 175 (2012).

[35] D. E. Kharzeev and E. M. Levin, Color Confinement and Screening in the θ Vacuum of QCD, Phys. Rev. Lett. **114**, 242001 (2015).

[36] D. de Florian, R. Sassot, and M. Stratmann, Global analysis of fragmentation functions for pions and kaons and their uncertainties, Phys. Rev. D **75**, 114010 (2007).

[37] D. Kharzeev and E. Levin, Manifestations of high density QCD in the first RHIC data, Phys. Lett. B **523**, 79 (2001).

[38] I. Balitsky, Operator expansion for high-energy scattering, Nucl. Phys. **B463**, 99 (1996); Factorization and high-energy effective action, Phys. Rev. D **60**, 014020 (1999); Y. V. Kovchegov, Small-x F_2 structure function of a nucleus including multiple Pomeron exchanges, Phys. Rev. D **60**, 034008 (1999).

[39] C. Contreras, E. Levin, and I. Potashnikova, CGC/saturation approach: A new impact-parameter dependent model, Nucl. Phys. **A948**, 1 (2016).

[40] A. H. Rezaeian, M. Siddikov, M. Van de Klundert, and R. Venugopalan, Analysis of combined HERA data in the impact-parameter dependent saturation model, Phys. Rev. D **87**, 034002 (2013).

[41] E. Levin and K. Tuchin, Solution to the evolution equation for high parton density QCD, Nucl. Phys. **B573**, 833 (2000).

[42] F. D. Aaron *et al.* (H1 and ZEUS Collaborations), Combined measurement and QCD analysis of the inclusive $e^\pm p$ scattering cross sections at HERA, J. High Energy Phys. 01 (2010) 109.

[43] M. Froissart, Asymptotic behavior and subtractions in the mandelstam representation, Phys. Rev. **123**, 1053 (1961); A. Martin, Scattering Theory: Unitarity, Analiticity and Crossing, *Scattering Theory: Unitarity, Analiticity and Crossing*, Lecture Notes in Physics (Springer-Verlag, Berlin-Heidelberg-New-York, 1969).

[44] E. Gotsman and E. Levin, CGC/saturation approach: Re-visiting the problem of odd harmonics in angular correlations, Eur. Phys. J. C **78**, 792 (2018).

[45] C. Contreras, E. Levin, and R. Meneses, Non linear evolution: Revisiting the solution in the saturation region, J. High Energy Phys. 10 (2014) 138.

[46] A. Kormilitzin, E. Levin, and S. Tapia, Geometric scaling behavior of the scattering amplitude for DIS with nuclei, Nucl. Phys. **A872**, 245 (2011).

[47] E. Levin and K. Tuchin, New scaling at high-energy DIS, Nucl. Phys. **A691**, 779 (2001); Nonlinear evolution and saturation for heavy nuclei in DIS, Nucl. Phys. **A693**, 787 (2001).

[48] D. Kharzeev and M. Nardi, Hadron production in nuclear collisions at RHIC and high density QCD, Phys. Lett. B **507**, 121 (2001).

[49] D. Kharzeev, E. Levin, and M. Nardi, Color glass condensate at the LHC: Hadron multiplicities in pp, pA and AA collisions, Nucl. Phys. **A747**, 609 (2005).

[50] D. Kharzeev, E. Levin, and L. McLerran, Parton saturation and $N_{(part)}$ scaling of semihard processes in QCD, Phys. Lett. B **561**, 93 (2003).

[51] D. Kharzeev, E. Levin, and M. Nardi, QCD saturation and deuteron nucleus collisions, Nucl. Phys. **A730**, 448 (2004); Erratum **A743**, 329 (2004).

[52] D. Kharzeev, E. Levin, and M. Nardi, The Onset of classical QCD dynamics in relativistic heavy ion collisions, Phys. Rev. C **71**, 054903 (2005).

[53] R. J. Glauber, in *Lectures on Theoretical Physics*, edited by , W. E. Brittin and L. G. Duham (Intersciences, New York, 1959), Vol. 1; Cross sections in deuterium at high energies, Phys. Rev. **100**, 242 (1955).

[54] M. L. Miller, K. Reygers, S. J. Sanders, and P. Steinberg, Glauber modeling in high energy nuclear collisions, Annu. Rev. Nucl. Part. Sci. **57**, 205 (2007).

[55] D. Kharzeev, C. Lourenco, M. Nardi, and H. Satz, A quantitative analysis of charmonium suppression in nuclear collisions, Z. Phys. C **74**, 307 (1997).

[56] ALICE Collaboration, Centrality determination in heavy ion collisions, CERN Report No. ALICE-PUBLIC-2018-011, 2018.

[57] A. H. Mueller, Nuclear A dependence near the saturation boundary, Nucl. Phys. **A724**, 223 (2003).

[58] D. Kharzeev, E. Levin, and L. McLerran, Parton saturation and $N_{(part)}$ scaling of semihard processes in QCD, Phys. Lett. B **561**, 93 (2003).

[59] A. H. Mueller, Parton saturation at small x and in large nuclei, Nucl. Phys. **B558**, 285 (1999).

[60] E. M. Levin and M. G. Ryskin, The Hadron-nucleus interaction in QCD at high-energy, Nucl. Phys. **B304**, 805 (1988).

[61] R. Abdul Khalek, J. J. Ethier, and J. Rojo, Nuclear parton distributions from lepton-nucleus scattering and the impact of an electron-ion collider, Eur. Phys. J. C **79**, 471 (2019), and references therein.

[62] V. A. Abramovsky, V. N. Gribov, and O. V. Kancheli, Character of inclusive spectra and fluctuations produced in inelastic processes by multi-pomeron exchange, Yad. Fiz. **18**, 595 (1973) [Sov. J. Nucl. Phys. **18**, 308 (1974)].

[63] E. Gotsman, E. Levin, and I. Potashnikova, CGC/saturation approach: secondary reggeons and $\rho = \mathrm{Re}/\mathrm{Im}$ dependence on energy, Phys. Lett. B **786**, 472 (2018); , CGC/saturation approach: soft interaction at the LHC energies, Phys. Lett. B **781**, 155 (2018).

[64] K. Aamodt et al. (ALICE Collaboration), Suppression of charged particle production at large transverse momentum in central Pb–Pb collisions at $\sqrt{s_{\mathrm{NN}}} = 2.76$ TeV, Phys. Lett. B **696**, 30 (2011).

[65] B. Abelev et al. (ALICE Collaboration), Centrality dependence of charged particle production at large transverse momentum in Pb–Pb collisions at $\sqrt{s_{\mathrm{NN}}} = 2.76$ TeV, Phys. Lett. B **720**, 52 (2013).

[66] J. Adam et al. (ALICE Collaboration), Centrality Dependence of the Charged-Particle Multiplicity Density at Mid-rapidity in Pb-Pb Collisions at $\sqrt{s_{\mathrm{NN}}} = 5.02$ TeV, Phys. Rev. Lett. **116**, 222302 (2016).

[67] S. Acharya et al. (ALICE Collaboration), Transverse momentum spectra and nuclear modification factors of charged particles in pp, p-Pb and Pb-Pb collisions at the LHC, J. High Energy Phys. 11 (**2018**) 013.

[68] G. Aad et al. (ATLAS Collaboration), Measurement of the jet fragmentation function and transverse profile in proton-proton collisions at a center-of-mass energy of 7TeV with the ATLAS detector, Eur. Phys. J. C **71**, 1795 (2011).

[69] Z. B. Kang, X. Liu, F. Ringer, and H. Xing, The transverse momentum distribution of hadrons within jets, J. High Energy Phys. 11 (2017) 068.

[70] E. Braaten and R. D. Pisarski, Soft amplitudes in hot gauge theories: A general analysis, Nucl. Phys. **B337**, 569 (1990).